

PAPER

World's first application of a self-deployable mechanism based on shape memory polymer composites in Mars explorations: ground-based validation and on-Mars qualification

To cite this article: Dou Zhang et al 2022 Smart Mater. Struct. 31 115008

View the article online for updates and enhancements.

You may also like

- Boron nitride-based shape memory polymers for spatially targeted ultrasound actuation
- Jiaxin Xi, David L Safranski, Reza Mirzaeifar et al.
- Three-dimensional constitutive model of woven fabric-reinforced shape memory polymer composites considering thermal residual stress
- Seok Bin Hong, Joon Hyeok Jang, Haedong Park et al.
- Modeling the shape memory and strength properties of fiber-reinforced shape memory polymer composite laminates
 Hao Zeng, Jianhua Liu, Zhimin Xie et al.



Smart Mater. Struct. 31 (2022) 115008 (13pp)

https://doi.org/10.1088/1361-665X/ac93d1

World's first application of a self-deployable mechanism based on shape memory polymer composites in Mars explorations: ground-based validation and on-Mars qualification

Dou Zhang¹, Liwu Liu¹, Pengfei Xu¹, Yinzhong Zhao², Qifeng Li³, Xin Lan³, Fenghua Zhang³, Linlin Wang³, Xue Wan³, Xin Zou⁴, Chengjun Zeng¹, Xiaozhou Xin¹, Wenxu Dai¹, Ying Li⁴, Yanchun He², Yanju Liu^{1,*} and Jinsong Leng^{3,*}

E-mail: yj_liu@hit.edu.cn and lengjs@hit.edu.cn

Received 22 April 2022, revised 5 July 2022 Accepted for publication 21 September 2022 Published 11 October 2022



Abstract

Mars is believed to contain signs of the ancient life and to be the future of humankind. Deep space explorations on Mars have received extensive attention from the scientific and engineering communities. An ancient papyrus scroll-inspired mechanism to deploy the national flag after landing is proposed in this paper. Firstly, a papyrus scroll-inspired structure folded and deployed by shape memory polymer composites (SMPCs) was designed. The material was characterised by both thermodynamic analysis and static mechanical tests. Then, computational modal analysis was completed with material parameters at 25 °C, 55 °C and 85 °C to investigate the temperature effect. Besides, ground-based engineering validations were conducted, including vibration, shock and acceleration tests, as well as deployment verification. Natural frequencies obtained from vibration agreed well with that calculated from simulation. Regular and vacuum deployments showed differences but were both acceptable. Additionally, release reliability greater than 99.99% was obtained through repeated experimental data. Finally, on-Mars qualification was completed with China's Tianwen-1 mission, with images of the deployed five-star red flag transmitted by the Zhurong rover. It is the world's first validation of self-deployable mechanism based on SMPCs in deep space, and further applications can be expected.

Keywords: shape memory polymer composites, self-deployable structures, vacuum deployments, release reliability evaluation, Tianwen-1 mission

(Some figures may appear in colour only in the online journal)

¹ Department of Astronautical Science and Mechanics, Harbin Institute of Technology, Harbin 150001, People's Republic of China

² Science and Technology on Vacuum Technology and Physics Laboratory, Lanzhou Institute of Technology, Lanzhou 730000, People's Republic of China

³ Centre for Composite Materials and Structures, Harbin Institute of Technology, Harbin 150080, People's Republic of China

⁴ Beijing Institute of Spacecraft System Engineering, Beijing 100094, People's Republic of China

^{*} Authors to whom any correspondence should be addressed.

1. Introduction

Deep space exploration, an extraordinary voyage in the solar system, galaxies, and universe, has evolved from early flybys and orbiters to planetary landing platforms and spacecraft probes [1, 2]. More than three billion years ago, Mars had a habitable extraterrestrial environment with a warm, humid climate, a strong magnetic field, a dense atmosphere, and other conditions that might support life. Whether this process occurred on Mars is the key to answering whether we are alone in the universe. Besides, reusable rockets and human-crewed spacecraft have been developed successfully for the long-term goal of the Mars migration. Therefore, Mars explorations are necessary for large-scale human migration [3]. There were three Mars exploration missions in 2020: the United Arab Emirates Hope Mars orbiter [4], the Chinese Tianwen-1 Mars probe [5] and the American Perseverance Mars rover [6]. Due to the lack of scientific foundations for Mars explorations, the development of all three payloads and the final assembly of the Hope was finished by American research institutions. The Tianwen-1 was developed by Chinese researchers independently. It carried out circumnavigation, landing and roving in one mission. The Perseverance, the most advanced Mars rover, functioned as a robotic geologist, collecting and storing geological samples that might contain evidence of life on Mars.

Shape memory polymers (SMPs) are typical smart materials that can maintain a temporary configuration and recover their original shape under certain stimuli such as heat, light, electric and magnetic fields etc [7]. The characteristics of self-deployable, low-density, and low-cost give rise to many promising applications in aerospace. However, the relatively low strength and stiffness have restricted their popularisation because they cannot be used for load-bearing systems. Composites reinforced by filament or fabric can significantly improve mechanical properties. Of them, the carbon fibre fabric is preferable due to its advantages of low density, high modulus, and good thermal and electrical conductivities [8, 9]. Therefore, carbon fibre reinforced shape memory polymer composites (SMPCs) have spread their applications to versatile forms, such as hinges, booms, solar arrays, and antennas [10-12].

Segregation apparatuses and deployable structures can significantly enrich the function and improve the space utilisation of the spacecraft, thereby supporting Mars explorations. The release device can be designed in various forms as the functional part for these deformable mechanisms. One of the most widespread types is explosive bolts. Three types of them have been contrived: piston type [13], shear type [14] and ridge cut type [15–17]. They have considerable loading capacity and extensive flight experiences, while the pyroshock and pyrotechnic pollution restrict their development. Thus, non-explosive actuators (NEAs) have emerged, especially for instruments with a sensible response to shock and vibration or contamination. Among NEAs, those exploiting shape memory materials, including shape memory alloys [18] (SMAs), SMPs and SMPCs, have attracted much attention. The release devices based on SMAs [19, 20] are ideal substitutions for explosive bolts with the advantages of repetition without deterioration and eliminating the volatile risk in storage and manipulations. However, their limited deformation capacity is a restriction.

In comparison, SMPCs are more suitable for applications with weight reduction and large deformation demands. In 2003, a shockless thermally actuated release nut was presented by Gall et al [21]. The release nut comprised two cylinders made of elastic memory composites, another name for SMPCs. They provided redundant options by enlarging the inner cylinder and shrinking the outer one simultaneously. Hereafter, the 'lotus', 'eight paws', and 'bamboo' release devices, which were also in the two-cylinder architecture, were put forward in 2015 by Wei et al [11] The modal characteristics and recovery properties were demonstrated. Zhao et al [22] went further by inheriting the two-cylinder structure but utilising the circumferential grooves to produce the latching force. Another configuration different from this two-cylinder pattern was proposed in 2020 [23]. SMPCs in this work were in a bent shape and hooked to a connector on the deployable panel. Besides, the heating system was different from resistor heaters made of constantan [24]. It adopted a flexible heater using the screen-printed technique for a coordinated deformation.

Landing is the most challenging task in Mars explorations, and usually, the exhibition of some vital information such as the national flag is necessary. However, the existing solution is to paste or print the flag on the lander. In 2008, the American flag printed on the Phoenix deck was about three feet above the Martian surface [25]. In 2013, the Chang'e 3 mission brought two Chinese flags to the moon, one was on the lander, and the other was on the Yutu rover [26]. In the Curiosity mission, the American flag medal was located on one of the four mobile swing arms of the rover [27] and was also found on the payload fairing [28]. In 2020, the American flag was printed on a plate located at the bottom of the rover's remote sensing mast and taken by the Perseverance rover to Mars again [29]. It can be seen that the national flag demonstration is an essential and meaningful task. Nevertheless, these approaches adopted craft's coating flags which were usually tiny and blurred due to the restriction of the plane on which they were printed.

It is possible for flags to flutter on Mars because the Martian wind has been proven by several pieces of literature [30, 31]. Therefore, to address the aforementioned limitations, we propose an ancient papyrus scroll-inspired mechanism released by SMPCs for a dynamic and clear flag demonstration. The mechanism comprises five parts: two SMPC devices, a national flag, an Al rod, two shoulders and two connectors. This paper is documented in the sequence of structure design and fabrication, finite element analysis, ground-based engineering validation, and on-Mars qualification. First, the architecture of the mechanism was proposed, with its working principle illustrated. Then, the mechanical properties of SMPCs were obtained from dynamic mechanical analysis and static tensile tests. Besides, ground-based engineering validation was conducted. Modal characteristics were analysed by both simulation and vibration tests. Deployments were carried out at normal temperature and pressure and in a vacuum chamber. Additionally, release reliability was also studied, and specimens undergoing multiple usages were characterised by a scanning electron microscope (SEM). Finally, on-Mars qualification was achieved in China's Tianwen-1 mission.

2. Experimental

An ancient papyrus scroll-inspired mechanism released by SMPC devices was proposed to deploy the national flag after landing on Mars in figure 1. It comprises five parts: two SMPC devices, a polyimide (PI) based national flag, an Al rod (tube hollowed for weight reduction), two connectors and two shoulders. The flag and SMPC devices were installed on the Mars landing platform through connectors. The Al rod, glued to the bottom of the flag, acted as a reel for folding. The flag pattern was concealed by rolling the flag along the Al rod, and then they were latched by bent SMPC devices. Two shoulders were assembled to the Al rod through threads to limit the axial displacement. After landing, the flag would be stretched by gravity by powering resistor heaters attached to SMPC devices to activate shape memory recovery. The preliminary demands for applications are listed in table 1. The low temperature of -70 °C was not cold enough for Mars but was limited by the vacuum equipment. It was acceptable in practice because the trigger for shape memory recovery could be artificially determined. The environmental temperature returned by sensors was also a reference for activating the deployment.

In this work, the material used was the epoxy-based SMP developed by Jinsong Leng's group [32]. The effect of γ -radiation and automatic oxygen on this epoxy-based polymer has been investigated [33, 34]. The results of dynamical and static mechanical tests and shape memory examination empower the material with the potential in aerospace structures. This polymer has been further validated as suitable for aerospace applications as a sunlight-stimulated substrate in 2016 [35] and a flexible solar array system in 2019 [36]. The carbon fibre fabric (Torayca T300-3K, plain-weave fabric) was selected as the reinforcement. The mechanical and thermal properties of fibres are obtained from the supplier with the tensile strength of 3530 MPa, the tensile modulus of 230 GPa, coefficient of thermal expansion of -0.41α . $10^{-6} \,^{\circ}\text{C}^{-1}$, and thermal conductivity of 0.105 J (cm·s·°C)⁻¹ [37]. A three-step thermal curing process was performed at 80 °C for 3 h, 130 °C for 3 h, 150 °C for 5 h and a heating rate of 3 °C min⁻¹, approximately. The material preparation and fabrication details can be found in the literature [32].

2.1. Mechanical tests of SMPCs

2.1.1. Dynamic mechanical analysis. The shape memory polymer used in this work is thermal-induced, and the recovery will be aroused when the temperature rises to its glass transition temperature (T_g) . Therefore, in order to obtain a reference temperature for the deployments, we conducted the thermo-dynamic mechanical tests on an analyser (NETXSCH Instruments Q800, Germany) in tensile mode at a frequency of 2 Hz. Specimens with dimensions of 60 mm \times 5 mm \times 2 mm were tested at a heating rate of 3 °C min⁻¹ from 10 °C to 220 °C. The storage modulus and tangent delta were identified,

and the $T_{\rm g}$ was set to be the temperature corresponding to the peak value of the tangent delta.

2.1.2. Static tensile tests. Specimens for tensile tests were prepared according to the standard ASTM D3039 with a dimension of 250 mm \times 25 mm \times 2 mm. Coupons for temperature-dependent properties were conducted at 25 °C, 55 °C, 85 °C, 140 °C and 200 °C. The 55 °C and 85 °C were chosen by the upper bound in the spacecraft and an additional safety margin (+30 °C), respectively. The 140 °C and 200 °C were close to and above the $T_{\rm g}$ to investigate the mechanical performance during deployments. The tests at 25 °C were performed on a Zwick/Rolle 050 machine with a load cell of 50 kN at a tensile rate of 2 mm min⁻¹ until broken. In contrast, those at high temperatures were conducted on a Zwick-/Rolle 010 machine with a load cell of 10 kN at a tensile rate of 2 mm min^{-1} . The coupons for high-temperature experiments were first heated to the target temperature in a chamber and then left for 20 min for uniform thermal distribution. Poisson's ratios ν were calculated by the transverse strain ε_2 and axial strain ε_1 recorded by strain gauges in figure 2(a) as:

$$\nu = -\varepsilon_2/\varepsilon_1. \tag{1}$$

2.2. Computational modal analysis

To evaluate the mechanical properties of assembled mechanism packaged by SMPC devices, the ABAQUS was used to conduct the computational modal analysis. The finite element model following the design was created in figure 2(b), where the flag was developed by the shell part, and the others are solid parts. SMPC devices and Al rod were meshed by C3D8 elements with the 'Sweep' technique, and the flag was also meshed with the 'Sweep' technique but by S4 elements. Due to their complicated geometry, the connectors and shoulders were meshed by C3D4 elements with the 'Free' approach. The connections among all interfaces (connectors & SMPC devices, SMPC devices & flag, flag & Al rod, Al rod & shoulders) were realised by 'Tie' constraints. Besides, the upper surfaces of the two connectors were fixed in all directions as boundary conditions. Material properties were listed in table 2, same as materials used in physical structures, of which parameters of SMPCs were obtained from static tensile tests.

2.3. Ground-based engineering verification

2.3.1. Vibration, shock, and acceleration tests. The mechanism will undergo complex mechanical conditions during the launch and astronavigation. The sinusoidal and random vibrations, shock and acceleration tests were conducted to assess its mechanical response. The structure was tested in three directions, as shown in figure 3, where the setup and control plots were presented. These three directions were the same as that in the finite element analysis for vibration and shock tests. In contrast, for acceleration tests, the *Y* direction was replaced by a combined direction of *Y* and *Z* as the mission required. The black lines were actual control plots collected by the sensors

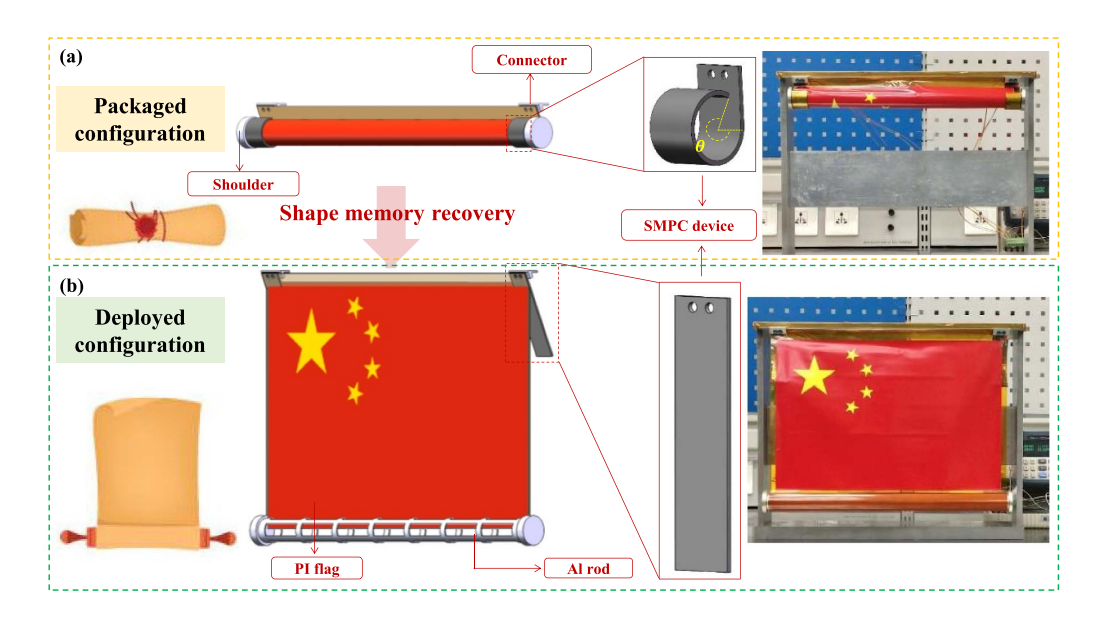


Figure 1. The ancient papyrus scroll-inspired mechanism, (a) packaged and (b) deployed configurations.

Table 1. Engineering requirements of the mechanism.

Description	Specification
Envelope size (packaged) Envelope size (deployed) Temperature range Actuation power Actuation time	400 mm × 60 mm × 55 mm 400 mm × 300 mm × 55 mm -70 °C-70 °C <40 W <15 min

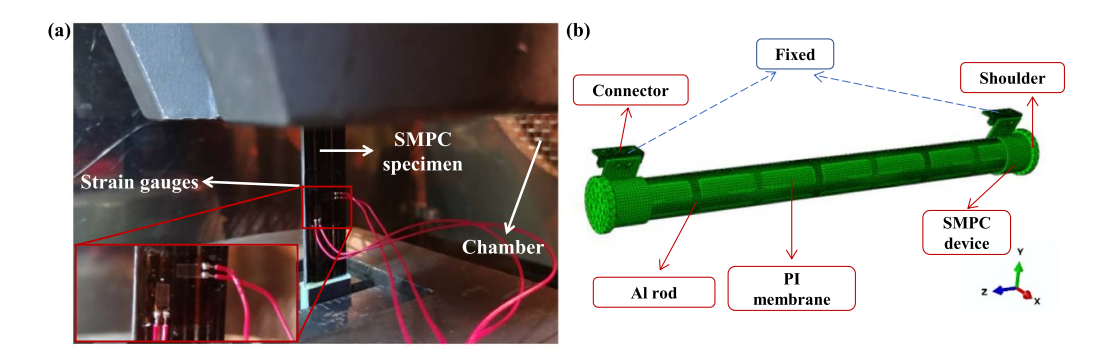


Figure 2. (a) Measurements for Poisson's ratio in tensile tests and (b) finite element model for modal analysis.

Table 2. Material parameters for the simulation.

Part	Mate	erial	Elastic modulus (GPa)	Poisson's ratio	Density (g cm ⁻³)
Release device	SMPC	25 °C	5.42	0.33	1.2
		55 °C	4.96	0.37	
		85 °C	4.63	0.4	
Flag	P	I	4	0.3	1.42
Al rod Connector	Α	.1	71	0.3	2.7
Shoulder					

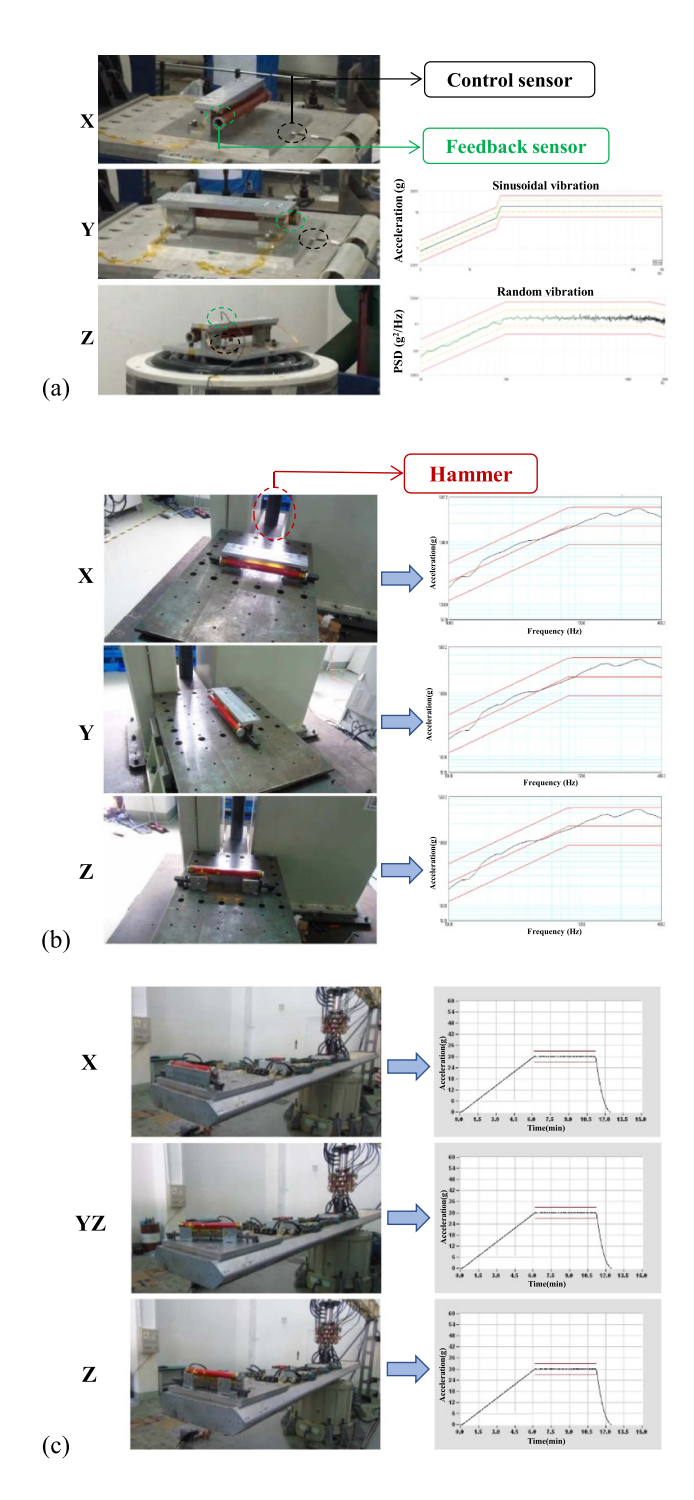


Figure 3. Experimental setups and control plots for (a) vibration, (b) shock and (c) acceleration tests.

fixed on the testing platform. These tests allow a tolerance of $\pm 10\%$, with red lines as the upper and lower limits. Vibration tests were conducted on an electrodynamic vibration system. An acceleration sensor was stuck to one of the SMPC devices to send the feedback signal. While for shock and acceleration tests, neither a feedback sensor nor foil gauge was used. Therefore, no data on the structure was collected. However, these tests were verified by checking the geometry and morphology

of the structure. Shock tests were performed on a pendulum impact test machine (SY14-100) with an 1800 g acceleration. The acceleration tests were carried out on a rotary arm centrifugal constant acceleration testing machine (Y53100-1AZF) with a 30 g acceleration for 5 min, where g is the gravitational acceleration and is approximately 9.8 m s⁻².

2.3.2. Ground-based deployment verification. The air pressure and environmental temperature play an essential role in the recovery of this thermal-induced SMPC. Except for normal pressure and temperature, 910 Pa and -70 °C, 25 °C, and 70 °C, referring to the actual mission conditions (in table 1), were also considered. Besides, the release reliability of SMPC devices is one of the most critical factors affecting the trustworthiness of the whole mechanism. Thus, repeated deployment tests were also carried out. The test samples selected for the reliability tests were consistent with the products for the actual flight mission. Ten test samples from the same batch as the flight article were used. Failure to release the flag after 10 min of power-on was deemed invalid. This failure could either be the degeneration of the shape memory effect or the invalidation of resistor heaters. The number of usages of a device was the number of normal releases. Therefore, the ground-based deployment could be divided into three parts: regular deployment, which indicated deployment in the normal pressure and temperature; vacuum deployment, which meant deployment in a vacuum chamber at 910 Pa and -70 °C, 25 °C, 70 °C; and repeated vacuum deployment which referred to multiple deployments in a vacuum chamber at 910 Pa and -70 °C until failure. The deployments were activated by resistor heaters attached to SMPC surfaces, powered by 28 V DC. The SMPC release device in a regular deployment was also monitored by a thermal infrared imager (Jenoptik InfraTec, Dresden, Germany) to record the heat distribution.

2.4. Morphology observation of SMPC devices

The large-angle bending and multiple usages could cause damage to SMPC devices at different levels. Among these damages, some were easy to inspect, such as buckling of carbon fibres or severe delamination, while others were hard to observe on the macroscopic scale. Therefore, a SEM was used to observe the morphology of SMPC devices. Internal surfaces (fibre microbuckling) and profiles (delamination) of bent devices were detected. Additionally, the first, fifth, tenth and twentieth-shaped devices were selected to conduct the morphology observation to investigate the progressive damage from repeated usage.

3. Results and discussion

3.1. Mechanical properties of SMPCs

3.1.1. Thermo-dynamic properties. The storage modulus and tangent delta of SMPCs as a function of temperature are depicted in figure 4(a). It is observed that the curve of storage

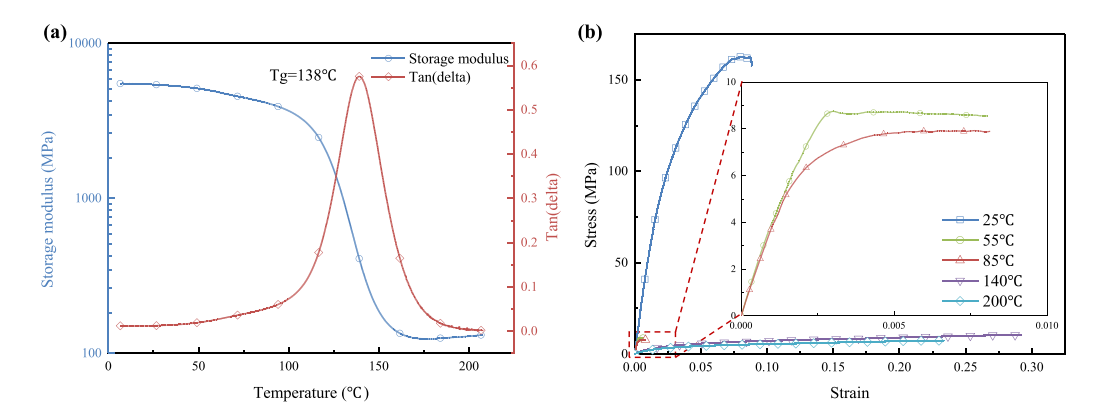


Figure 4. Mechanical properties of SMPCs, (a) storage modulus and tangent delta versus temperature curves from dynamic mechanical analysis and (b) stress versus strain curves from static tensile tests.

Table 3. Mechanical properties under different temperatures of SMPCs.

Temperature (°C)	Storage modulus (GPa)	Tensile modulus (GPa)	Poisson's ratio
25	6.4	5.42	0.33
55	5.3	4.96	0.37
85	4.7	4.63	0.40
140	0.37	0.116	0.42
200	0.13	0.103	0.42

modulus can be partitioned into three regions: the glassy state, the glass transition region, and the rubbery state, indicating that this material exhibits variable stiffness with temperature. The storage modulus demonstrates a sharp decrease during the glass transition region, from about 6430 MPa in the glassy state to only 150 MPa in the rubbery state, showing an approximate 42 times reduction. Tangent delta is the ratio of the dynamic loss modulus to the storage modulus, which reflects the viscosity of the material. The temperature corresponding to the peak value of this curve is about 138 °C, which is regarded as $T_{\rm g}$. Therefore, in order to trigger the self-deployments, the SMPC is required to be heated up to 138 °C to drive the shape memory recovery. More details can be found in the infrared images in regular deployments.

3.1.2. Static tensile properties. The mechanical properties at five key temperatures are listed in table 3, where the tensile modulus is calculated by the slope of the initial straight line of the stress versus strain curves from tensile tests in figure 4(b). The tensile modulus decreases slightly with increasing temperature below 85 °C, from 5.42 GPa to 4.63 GPa. It decreases sharply to 0.116 GPa around $T_{\rm g}$ and 0.103 GPa at 200 °C, showing a two-order-of-magnitude drop. This temperaturedependent stiffness is consistent with the storage modulus from the dynamic mechanical analysis in figure 4(a). The discrepancy between these two moduli could be caused by the loading rate and lies in the essence of the viscoelastic property of shape memory epoxy resin. Poisson's ratios increase with the temperature from 0.33 at 25 °C to 0.42 at 200 °C. The tensile strength reduces by about 95%, from 164 MPa at 25 °C to 10.39 MPa at 140 °C and 7.35 MPa at 200 °C. However, the platforms at 55 °C and 85 °C do not represent strength because no damage was found between the two grips. It was caused by scratches on the clamping end of these coupons due to the limitation of pneumatic fixtures. These results are acceptable because the purpose of these tests is to provide material parameters for the computational modal analysis, where only the tensile modulus and Poisson's ratio are used.

3.2. Ground-based engineering validation

It is necessary to investigate the shape fixation characteristics before engineering validation because the viscoelastic property makes the temperature and time important to the SMPC's configuration. Curved devices were put into a drying oven with setting temperatures of 25 °C, 55 °C and 85 °C, respectively, for 96 h. The results described in figure 5(a) show a temperature-sensitive feature. The radius of curvature is invariable at 25 °C within 96 h, while it presents a slight increase at 55 °C and 85 °C. For devices at 55 °C, a 0.08 mm augment is observed when it lasts for 24 h and remains almost unchanged thereafter. A similar pattern is detected at 85 °C with the radius increased by 0.26 mm. It is drawn that the device undergoes a relatively noticeable change in the first 24 h while maintaining a stable configuration afterwards. Release devices with a stable shape after 96 h of creep, even at 85 °C, can guarantee a reliable mechanical latching for the mechanism, and it will be verified by vibration tests.

3.2.1. Modal characteristics. The first four order natural frequencies at 25 °C, 55 °C and 85 °C are predicted by finite element simulation, and the results at 25 °C are validated by vibration tests at room temperature. Consistency of comparison verifies the reliability of the simulation method, and results at high temperatures. The vibration modes at three temperatures are similar, so we take the results at 25 °C for illustration. As shown in figure 5(b), the first-order mode shows an outward swing along the X-axis. The second mode combines torsion along the Z-axis and movement along the Y-axis. The third offers a combination of torsion along the Z-axis

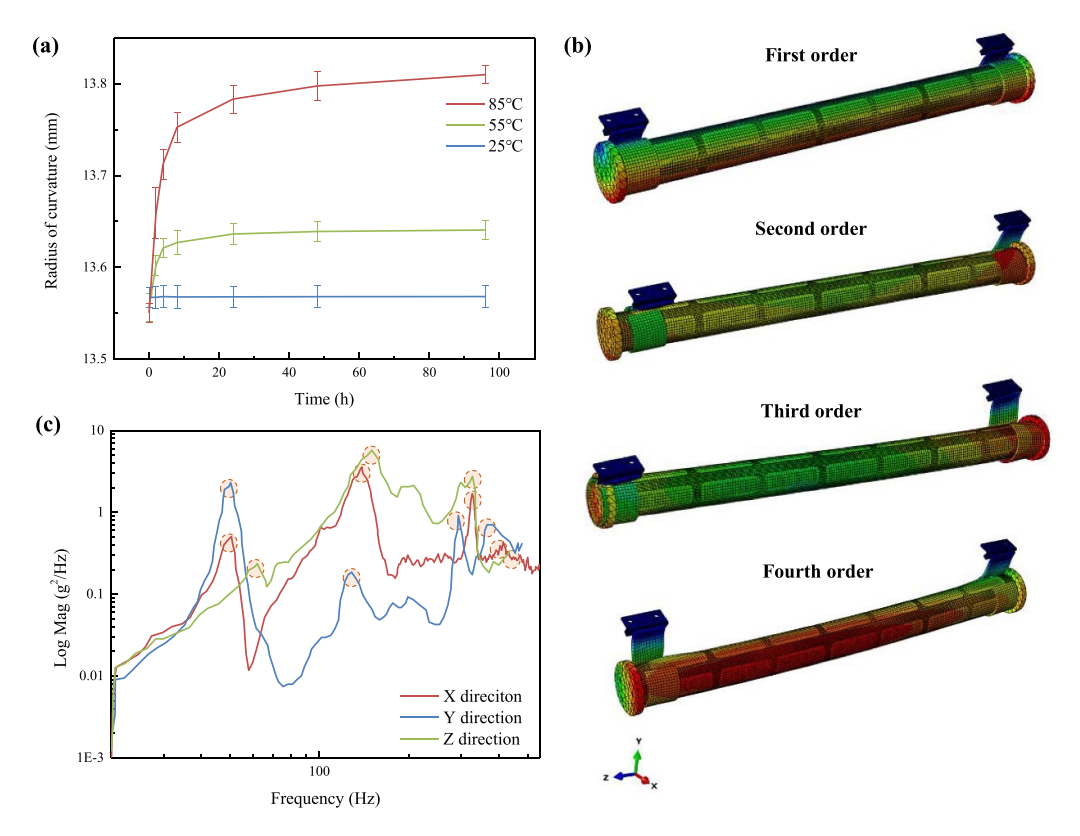


Figure 5. (a) The radius of curvature versus time at different temperatures $(25 \,^{\circ}\text{C}, 55 \,^{\circ}\text{C} \text{ and } 85 \,^{\circ}\text{C})$, (b) the first four order modes of the mechanism using SMPC's tensile parameters at $25 \,^{\circ}\text{C}$ and (c) responses of feedback sensor from random vibration in three directions at $25 \,^{\circ}\text{C}$ with resonance frequencies circled in orange.

Table 4. The first four-order natural frequencies of the folded mechanism from simulation.

		Natural freq	uencies (Hz)	
Temperature ($^{\circ}$ C)	1st	2nd	3rd	4th
25	53.67	148.36	196.25	198.18
55	50.96	141.51	188.11	189.79
85	48.34	134.70	180.01	181.50

and movement along the *Y*-axis. The fourth is a combination of rotations along the opposite *Y*-axis and *Z*-axis. The first four-order natural frequencies listed in table 4 demonstrate a slight decrease as the temperature increases, which is caused by the reduction of the SMPC's modulus. Compared with data at 25 °C, only about 10% reduction occurs at 85 °C, which infers that the mechanism can maintain a reliable folded architecture at this temperature.

Random vibration results are depicted in figure 5(c), of which the specimens suffered 96 h of creep at 85 °C in advance, with a 0.26 mm augment in radius. Although curves of signal from feedback sensor versus frequency show variable shapes in three directions, the local peaks circled in orange are very close to each other, representing resonance frequencies. The first four-order natural frequencies are determined by the averaged resonance frequencies in three directions. The results in table 5 show good agreement with the simulation data, with an acceptable error which is inevitable. This is due to the previous creep, as well as the simplification of the finite element model and experimental errors. As for sinusoidal vibration, the

first-order natural frequency is 53.3 Hz on average, agreeing well with the simulation and random vibration results. The higher-order frequencies are not received because the tests are limited by the frequency range. Further, the influence of shape memory cycles on the natural frequency is also investigated by sinusoidal vibrations. The results reveal that after undergoing 20 shape memory cycles, the mechanism's first-order natural frequency is 50.91 Hz, showing a 4.48% decline. This decrease is expected because shape memory cycles could cause microscale damage which will be demonstrated in the following subsection, weakening the latching performance of SMPC devices.

The geometry and morphology of the structure are examined after shock and acceleration tests, with no deformation or damage found. Besides, resistor heaters adhere well to SMPC devices with little change in resistance. Although no data are collected directly in these tests, the observations effectively indicate that the mechanism has excellent performance under shock and acceleration conditions, with neither mechanical nor electrical damage caused.

			Natural frequencies (Hz)			
Test		1st	2nd	3rd	4th	
Si	mulation		53.67	148.36	196.25	198.18
Random vibration	Direction	X	50.66	138.17	221.48	297.57
		Y	50.44	128.05	196.92	258.15
		Z	61.58	150.62	218.68	306.73
	Ave	rage	54.23	138.95	212.36	287.48
	Relatively	error (%)	1.04	-6.9	8.21	45.06
Sweep sine	Direction	X	49.68			
		Y	52.57	_	_	_
		Z	57.64	_	_	_
	Ave	rage	53.3			
	Relatively	error (%)	0.7	_	_	

Table 5. First four-order natural frequencies of the mechanism at 25 °C.

After comprehensive considerations, including creep tests and modal analysis of both simulation at high temperatures and vibration after creep, the mechanism assembled by SMPC devices is validated to have a satisfying mechanical response, even at relatively high temperatures and after 20 shape memory cycles.

3.2.2. Deployment demonstration. The deployments are triggered by the shape memory recovery of SMPC devices. The regular and vacuum deployments at -70 °C powered by 28 V DC are demonstrated. Firstly, the regular deployment and the corresponding heat maps of an SMPC device during the recovery process are shown in figures 6(a) and (b), respectively. The recovery starts from about 45 s when the rolled-up flag looks loose. The temperature in the middle of the resistor heater is the highest and is about 190 °C, 52 °C higher than $T_{\rm g}$ in figure 4(a). This is consistent with our previous work where the arousing temperature of the shape memory recovery is higher than the $T_{\rm g}$ [23]. The heat is concentrated in the middle, while the temperature in the margins is about 30 °C lower. Besides, the temperature monitored is the surface temperature of the heater. In fact, it can be seen in figure 6(b) at 45 s that the temperature on the inner surface of SMPC is about 60 °C lower than the heater. This uneven heat distribution delays the shape recovery but the superior thermal conductivity of carbon fibres can mitigate this impact. Therefore, the SMPC is regarded as having entered the glass transition region. Then at 70 s, the temperature in the middle rises to 230 °C, and SMPC devices show an obvious forward deformation. As the recovery continues, the temperature in the middle of the resistor heater is stable at 270 °C, and the Al rod begins to slide down under the action of gravity. Finally, the flag is fully unfolded at 102 s. At this time, the deployed SMPC devices are hidden behind, without any obstruction to the flag.

Unfortunately, such a detailed process cannot be recorded in vacuum deployments due to the limited field of view of the equipment. Therefore, images with SMPC devices framed in yellow before and after deployments are presented in figure 6(c). The unfolding takes 257 s, which is about 2.5-time longer than regular deployments because the environmental

pressure and temperature significantly weaken the heating performance and delay the recovery. It can be seen from the side view that a noticeable gap exists between the recovered SMPC devices and the unfolded flag, allowing the flag to flutter in the Martian breeze.

Further, vacuum deployments at different temperatures $(-70 \,^{\circ}\text{C}, 25 \,^{\circ}\text{C})$ and $70 \,^{\circ}\text{C})$ and power voltages $(21 \, \text{V}-32 \, \text{V})$ are presented in figure 6(d). It is observed that the release time is shortened regardless of whether the temperature or voltage rises. For instance, the release time stimulated by $21 \, \text{V}$ at $-70 \,^{\circ}\text{C}$ is $13.5 \, \text{min}$, while it reduces to $5.4 \, \text{min}$ at $70 \,^{\circ}\text{C}$, showing a 2.5-time drop. When the temperature is $-70 \,^{\circ}\text{C}$, the release times are $13.5 \, \text{min}$ and $1.8 \, \text{min}$ for those powered by $21 \, \text{V}$ and $32 \, \text{V}$, respectively, presenting a 7.5-time decline. In addition, when it is $-70 \,^{\circ}\text{C}$ and $21 \, \text{V}$, the release costs $13.5 \, \text{min}$, while the deployment completes at about $0.5 \, \text{min}$ for $70 \,^{\circ}\text{C}$ and $32 \, \text{V}$, showing a 27-fold reduction. The mechanism offers superior adaptability to ambient temperature and power supply.

For repeated vacuum deployments, the release time in figure 6(e) experiences a slight fluctuation but is still around 257 s. The repetition of the 'load at high temperatures-cooling while maintaining load-unload at low temperatures-recovery while heating' cycle does not significantly deteriorate releasing response. In contrast, the morphology demonstrates some changes. The bending morphologies in figure 7 show apparent fibre buckling in the highly strained inner surface. The SEM images suggest that the warp and fill yarns are no longer perpendicular to each other but at an about 120° angle, agreeing well with the macro morphology. Besides, delamination appears from the fifth bending, both from macroscopic and SEM observations. It becomes increasingly severe as shape memory cycles continue, and four layers emerge distinctly at the twentieth bending observed from the profile of SEM morphology. The matrix damage occurs from the tenth bending and is visible on a macroscale at the twentieth usage. The mechanical performance of the SMPCs with the progressive damage is characterised by sinusoidal vibrations with a 4.48% decline in the first-order natural frequency.

Experiments including the creep and modal analysis at different temperatures, and 20 shape memory cycles show

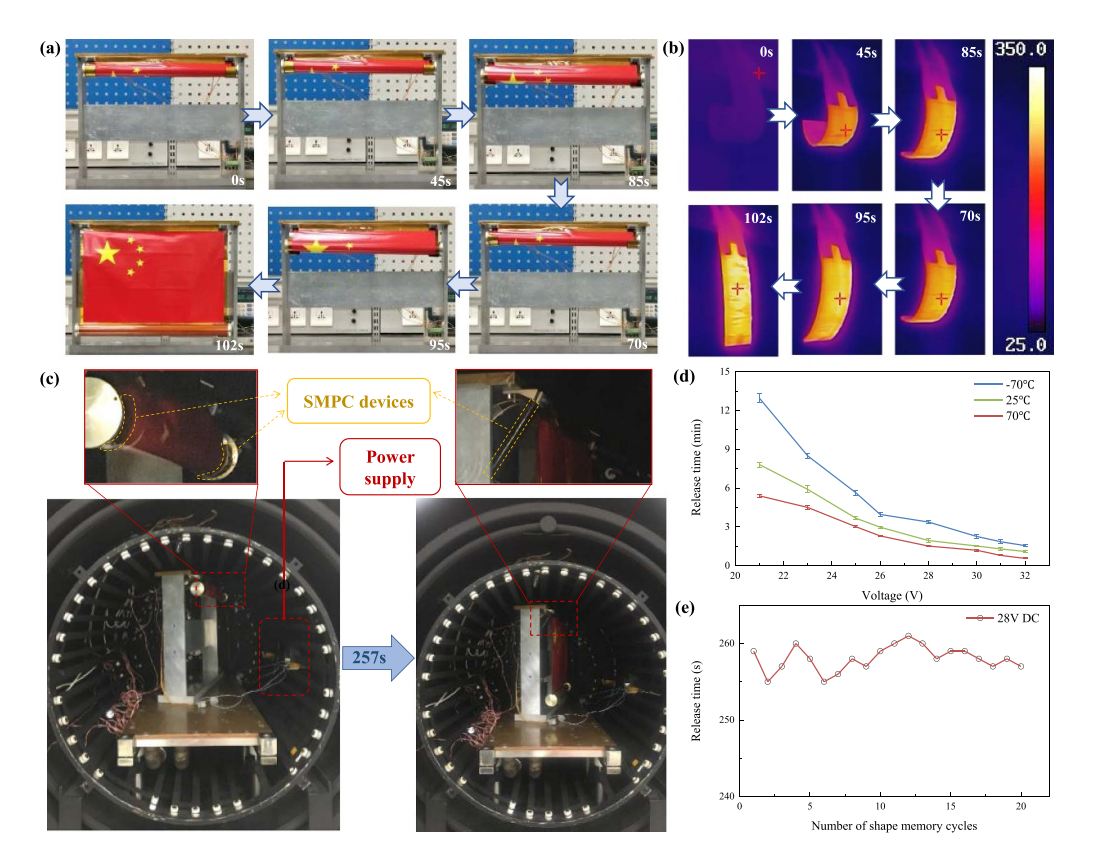


Figure 6. Deployment demonstration, (a) regular deployment, (b) the detailed heat maps of the SMPC device during the regular deployment, (c) vacuum deployment at $-70\,^{\circ}$ C, (d) release time of vacuum deployment under different temperatures and voltages and (e) release time of repeated vacuum deployments.

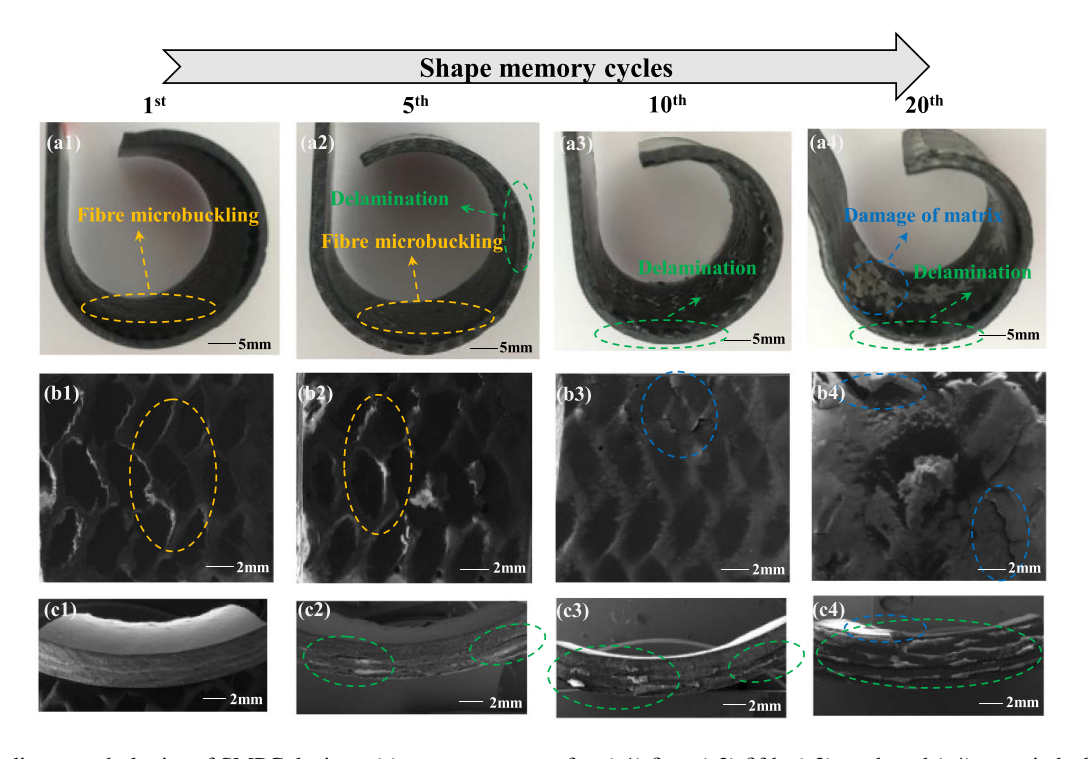


Figure 7. Bending morphologies of SMPC devices, (a) macrostructure after (a1) first, (a2) fifth, (a3) tenth and (a4) twentieth shape memory cycles; (b) inner surface from SEM after (b1) first, (b2) fifth, (b3) tenth and (b4) twentieth shape memory cycles; and (c) profile from SEM after (c1) first, (c2) fifth, (c3) tenth and (c4) twentieth shape memory cycles.

less than 10% variation. Therefore, it can be concluded that the mechanism has a reliable mechanical property assembled by SMPC devices, even at a relatively high environmental temperature (85 °C) and after multiple usages (20 cycles).

3.3. Release reliability evaluation

The release reliability evaluation assesses the probability that products complete the release function under specific conditions to meet the reliability requirements. Pyrotechnic devices are one-time operations in orbit. The result is either success or failure. Thus, they are usually evaluated based on a binomial distribution. Considering the repeatable characterisation of SMPC products, the metrological method can be used. The release reliability R is defined as the probability that SMPC devices complete one or more release functions under the specified test conditions, which is at $-70\,^{\circ}\text{C}$ and 910 Pa, and can be calculated as:

$$R = P\{N \geqslant 1\} \tag{2}$$

where N represents the number of usages and is a non-negative integer. A reasonable probability distribution assumption for N is the basis for effective reliability evaluation. Considering that N is a discrete random variable, and according to the engineering experience, for a batch of products with stable performance, the number of usages is concentrated on a specific value, and those far away from this value should be excluded. That is, when the number of uses N = k, the probability $P\{N = k\}$ first increases with k, and then drops when k approaches a specific range. This fits the Poisson distribution [38]:

$$p_k\{N=k\} = \frac{\lambda^k}{k!} e^{-\lambda} (k=0, 1, 2, ..., \lambda > 0)$$
 (3)

where p_k is the probability when N equals k, and λ is the Poisson distribution parameter, reflecting the average usages. The release reliability of SMPCs in orbit is:

$$R = P\{N \ge 1\} = \sum_{k=1}^{\infty} p_k = \sum_{k=1}^{\infty} \frac{\lambda^k}{k!} e^{-\lambda} = 1 - e^{-\lambda}.$$
 (4)

Therefore, several test samples are selected to obtain experimental data, estimating Poisson distribution parameters. Record the sum of experimental data obtained by n samples as T:

$$T = \sum_{i=1}^{n} N_i. \tag{5}$$

Then, for a given confidence coefficient $\gamma=1-\alpha$, the one-sided lower confidence limit λ_L of the Poisson distribution parameter λ is:

$$\lambda_{\rm L} = \frac{1}{2n} \chi_{\alpha}^2 (2T) \,. \tag{6}$$

Herein, $\chi^2_{\alpha}(2T)$ expresses the α quantile of the chi-square distribution [39] with the degree of freedom of 2T. Substituting

Table 6. Release reliability variation with confidential coefficient.

Confidence coefficient γ	Quantile α	One-sided lower confidence limit λ_L	Release reliability <i>R</i>
0.005	0.995	18.8059	>0.9999
0.025	0.975	19.6559	>0.9999
0.8	0.2	23.7518	>0.9999
0.9	0.1	24.4425	>0.9999
0.95	0.05	25.0228	>0.9999
0.975	0.025	25.5335	>0.9999
0.98	0.02	25.6868	>0.9999
0.99	0.01	26.1359	>0.9999

 λ_L instead of λ into the formula, the lower confidence limit of the release reliability can be obtained as:

$$R = 1 - e^{-\lambda_{\rm L}}. (7)$$

The number of test samples is 10 in this work, and the sum of experimental data T is:

$$T = \sum_{i=1}^{10} N_i (i = 1, 2, \dots n) = 228.$$
 (8)

The one-sided lower confidence limit λ_L and release reliability R varying with confidence coefficient γ are listed in table 6. It is found that the release reliability is always greater than 0.9999 regardless of the confidence coefficient. In other words, the mechanism can always meet the reliability requirements of aerospace applications (greater than 0.9999).

4. On-Mars functional qualification

This self-deployable flag mechanism is part of China's Tianwen-1 mission [5], which launched in July 2020 and arrived in Mars orbit in February 2021. On 22nd May 2021, the Zhurong rover and the landing platform separated from the Tianwen-1 orbiter and touched down. The deployment of the national flag of China was shown in figure 8 [40], which was sent back on 11th June 2021. The rover took these photos by dropping a camera attached to its belly about 10 m away from the landing platform. Figure 8(a) was taken at this time. Then the rover positioned itself next to the landing platform, and at this time, figure 8(b) was taken. The camera wirelessly transmitted these photos to the rover which sent them to Earth via the Tianwen-1 orbiter. Although the deployment process was not recorded, a deployed five-star red flag framed in red dashed lines in these two photos was clear and visible. The successful deployment has proven the papyrus scroll mechanism's mechanical and functional success. It is the world's first validation of SMPCs in deep space explorations after their successful verification in geosynchronous orbit in 2016 [35] and 2020 [36]. This smart material is expected to contribute to the following sample return programs from Mars and explorations to other deep spaces such as asteroids and Jupiter.

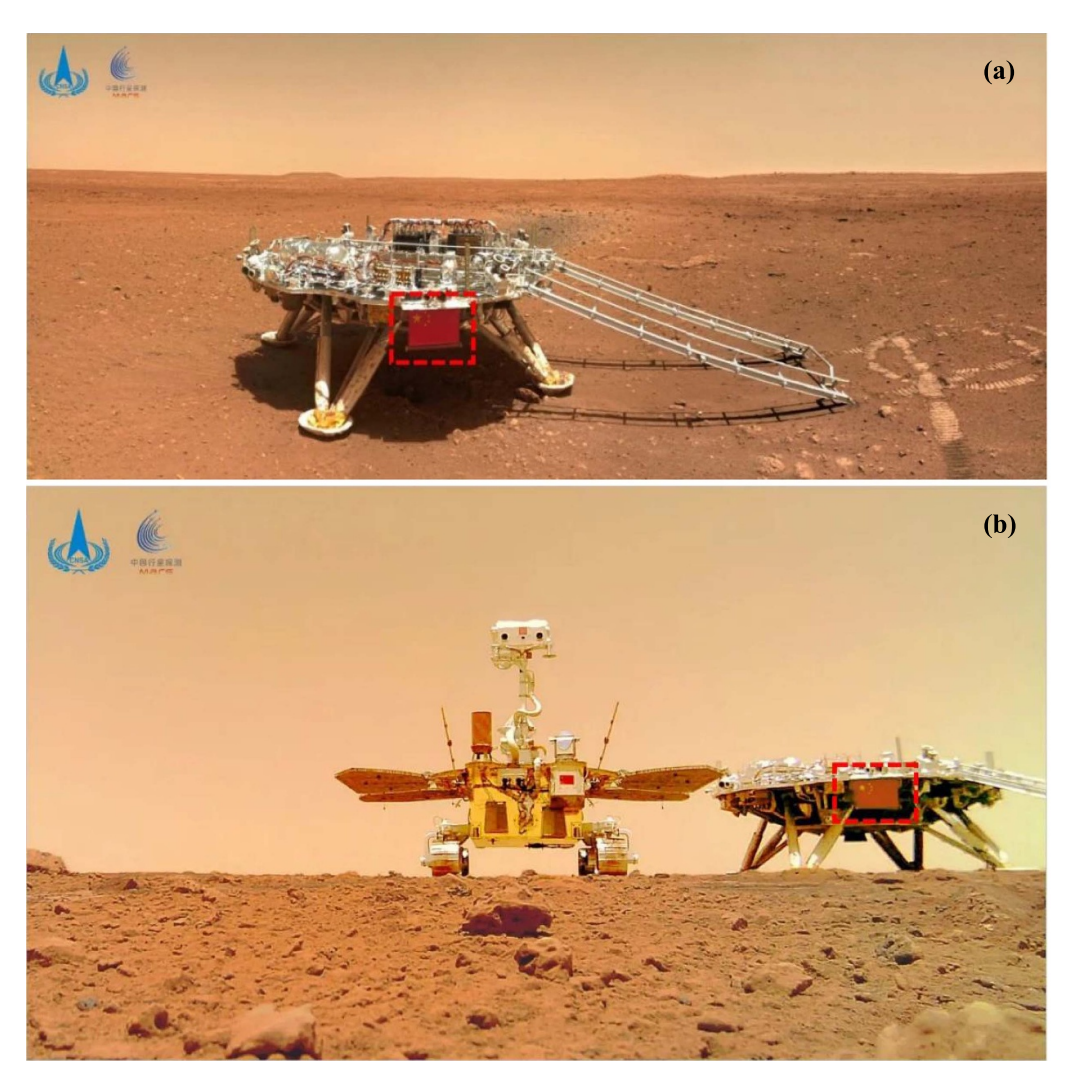


Figure 8. On-Mars qualification with the deployed national flag of China framed in red. Photos from the camera attached to the rover, (a) a side view of the Tianwen-1 landing platform and (b) the group photo of the Zhurong rover (left) and landing platform (right) Reproduced with permission from [40].

5. Conclusions

An ancient papyrus scroll-inspired self-deployable mechanism is proposed to demonstrate China's national flag in the Mars exploration. Ground-based engineering validation and on-Mars qualification in the Tianwen-1 mission are conducted, and several conclusions can be drawn. Firstly, release devices made of SMPCs, as the key to switch folded and deployed configurations, are characterised. The dynamic mechanical analysis shows three regions with the increase in temperature and gives the $T_{\rm g}$ (138 °C). Mechanical parameters are obtained by tensile tests, and then used in the computational modal analysis. The first-order natural frequencies at 55 °C and 85 °C from computational modal analysis decrease by 4.94% and 9.93%, respectively, compared with those at 25 °C. Besides, simulation results at 25 °C are compared with vibration data to validate the feasibility of the finite element method and the effectiveness of results at high temperatures. Besides, the creep effect of this macromolecular polymer is also taken into consideration. The radii of curvature increase by 0.08 mm and 0.26 mm after creeping for 96 h at 55 °C and 85 °C, respectively, of which the mechanical performance is evaluated by vibration tests. Additionally, ground-based deployment is conducted at normal temperature and pressure, and in a vacuum chamber. The mechanism possesses excellent adaptability, with release time varying from 0.5 min at -70 °C and 21 V to 13.5 min at 70 °C and 32 V. The release reliability is evaluated by 20 folded-deployed cycles, with reliability higher than 99.99%. Finally, the on-Mars qualification was successfully completed with China's first Mars exploration Tianwen-1 mission. This world's first validation of SMPCs in Mars explorations is a milestone, extending their applications from the geosynchronous orbit to deep space. More applications in versatile architectures with this smart material can be expected.

Data availability statement

The data that support the findings of this study are available upon reasonable request from the authors.

Acknowledgments

The authors would like to thank all members of the Smart Materials and Structures group at Harbin Institute of Technology and the China Academy of Space Technology. This work is supported by the Heilongjiang Touyan Innovation Team Program and the National Natural Science Foundation of China: Grant Nos. 11872020 and 12102107.

ORCID iDs

References

- [1] Nagy K 2019 Deep space exploration: the future challenge in engineering (NASA) (available at: https://core.ac.uk/ download/pdf/211015816.pdf) (Accessed 7 October 2021)
- [2] Bartone P T, Roland R, Bartone J, Krueger G, Sciaretta A and Johnsen B H 2019 Human adaptability for deep space exploration mission: an exploratory study *J. Hum. Perform.* Extreme Environ. 15 5
- [3] Zheng Y 2020 Mars exploration in 2020 Innovation 1 100036
- [4] Wadhi M A, Bonnici M and Handley W 2021 Pointing and alignment for the Emirates Mars mission 2021 IEEE Aerospace Conf. (50100) (Big Sky, MT: IEEE) pp 1–8
- [5] Zou Y et al 2021 Scientific objectives and payloads of Tianwen-1, China's first Mars exploration mission Adv. Space Res. 67 812–23
- [6] Farley K A et al 2020 Mars 2020 mission overview Space Sci. Rev. 216 1–41
- [7] Liu T, Zhou T, Yao Y, Zhang F, Liu L, Liu Y and Leng J 2017 Stimulus methods of multi-functional shape memory polymer nanocomposites: a review *Composities* A 100 20–30
- [8] Hong S B, Jang J H, Park H, Kim J-G, Goo N S and Yu W-R 2019 Three-dimensional constitutive model of woven fabric-reinforced shape memory polymer composites considering thermal residual stress *Smart Mater. Struct.* 28 035023
- [9] Gao J, Chen W, Yu B, Fan P, Zhao B, Hu J, Zhang D, Fang G and Peng F 2019 Effect of temperature on the mechanical behaviours of a single-ply weave-reinforced shape memory polymer composite *Composities* B 159 336–45
- [10] Liu T Z, Liu L W, Yu M, Li Q, Zeng C, Lan X, Liu Y and Leng J 2018 Integrative hinge based on shape memory polymer composites: material, design, properties and application *Compos. Struct.* 206 164–76
- [11] Wei H Q, Liu L W, Zhang Z C, Du H, Liu Y and Leng J 2015 Design and analysis of smart release devices based on shape memory polymer composites *Compos. Struct.* 133 642–51
- [12] Li F, Liu L, Lan X, Zhou X, Bian W, Liu Y and Leng J 2016 Preliminary design and analysis of a cubic deployable support structure based on shape memory polymer composite *Int. J. Smart Nano Mater.* 7 106–18
- [13] Li Y H, Wang J C, Xiong S H, Cheng L, Wen Y and Li Z 2019 Numerical study of separation characteristics of piston-type explosive bolt *Shock Vib.* 2019 209279

- [14] Li Y H, Xiong S H, Li Y, Li X, Wen Y, Mu H and Li Z 2017 Identification of pyrotechnic shock sources for shear type explosive bolt *Shock Vib.* 2017 3846236
- [15] Lee J, Han J H, Lee Y and Lee H 2014 Separation characteristics study of ridge-cut explosive bolts *Aerosp. Sci. Technol.* 39 153–68
- [16] Lee J, Han J H, Lee Y and Lee H 2015 A parametric study of ridge-cut explosive bolts using hydrocodes *Int. J. Aeronaut Space Sci.* 16 50–63
- [17] Lee J, Hwang D H, Jang J K, Kim D J, Lee Y, Lee J R and Han J H 2016 Pyroshock prediction of ridge-cut explosive bolts using hydrocodes *Shock Vib.* 2016 1218767
- [18] Jani J M, Leary M and Subic A and Gibson M A 2014 A review of shape memory alloy research, applications and opportunities *Mater. Des.* 56 1078–113
- [19] Glucksberg A, Soul H and Yawny A 2018 Releasing systems for aerospace industry based upon shape memory alloys: characterisation of materials for actuators *Materia-Rio J.*
- [20] Nava N, Collado M and Cabas R 2014 New pin puller based on SMA technology for space applications J. Mater. Eng. Perform. 23 2712–8
- [21] Gall K, Lake M, Harvey J and Ricca E 2003 Development of a shockless thermally actuated release nut using elastic memory composite material AIAA/ASME/ASCE/AHS/ASC Structures, Structural Dynamics, & Materials Conf
- [22] Zhao H, Lan X, Liu L, Liu Y and Leng J 2019 Design and analysis of shockless smart releasing device based on shape memory polymer composites *Compos. Struct.* 223 110958
- [23] Zhang D, Liu L, Leng J and Liu Y 2020 Ultra-light release device integrated with screen-printed heaters for CubeSat's deployable solar arrays *Compos. Struct.* 232 111561
- [24] Lan X, Liu Y, Lv H, Wang X, Leng J and Du S 2009 Fiber reinforced shape-memory polymer composite and its application in a deployable hinge *Smart Mater. Struct.* 18 024002
- [25] Hoffman J H, Chaney R C and Hammack H 2008 Phoenix mars mission—the thermal evolved gas analyser J. Am. Soc. Mass Spectrom. 19 1377–83
- [26] Li C *et al* 2015 The Chang'e 3 mission overview *Space Sci. Rev.* **190** 85–101
- [27] NASA 2015 Curiosity's stars and stripes *Curiosity's Stars and Stripes—NASA Mars Exploration* (Accessed 30 June 2022)
- [28] Lakdawalla Emily 2018 Getting to Mars The Design and Engineering of Curiosity (Harland David Springer-Praxis Books in Space Exploration) (New York: Springer) pp 57–59
- [29] NASA 2020 Messages on Mars Perseverance rover (available at: https://mars.nasa.gov/mars2020/spacecraft/rover/ markings/) (Accessed 7 October 2021)
- [30] Gierasch P and Sagan C 1971 A preliminary assessment of Martian wind regimes *Icarus* 14 312–8
- [31] Nakamura Y and Anderson D L 2013 Martian wind activity detected by a seismometer at Viking Lander 2 site *Geophys*. *Res. Lett.* 6 499–502
- [32] Leng J, Wu X and Liu Y 2009 Effect of a linear monomer on the thermomechanical properties of epoxy shape-memory polymer Smart Mater. Struct. 18 095031
- [33] Leng J, Xie F, Wu X and Liu Y 2014 Effect of the γ-radiation on the properties of epoxy-based shape memory polymers *J. Intell. Mater. Syst. Struct.* **25** 1256–63
- [34] Tan Q, Li F, Liu L, Chu H, Liu Y and Leng J 2018 Effects of atomic oxygen on epoxy-based shape memory polymer in low earth orbit J. Intell. Mater. Syst. Struct. 29 1081–7
- [35] Li F, Liu L, Lan X, Pan C, Liu Y, Leng J and Xie Q 2019 Ground and geostationary orbital qualification of a

- sunlight-stimulated substrate based on shape memory polymer composite *Smart Mater. Struct.* **28** 075023
- [36] Lan X et al 2020 World's first spaceflight on-orbit demonstration of a flexible solar array system based on shape memory polymer composites Sci. China Technol. Sci. 63 1436–51
- [37] Toray CFA Inc T300 carbon fiber data sheet n.d.:6–7 (available at: www.toraycma.com/wp-content/uploads/T300-Technical-Data-Sheet-1.pdf.pdf) (Accessed 2 July 2022)
- [38] Sahai H and Khurshid A 1993 Confidence intervals for the mean of a Poisson distribution: a review *Biom. J.* 35 857–67
- [39] Lancaster H O and Seneta E 2005 Chi-square distribution Encyclopedia of Biostatistics 2nd edn, ed P Armitage and T Colton (New York: Wiley) p 2
- [40] China National Space Administration 2021 Deployed National Flag of China (available at: www.cnsa.gov.cn/n6758823/ n6758838/c6812123/content.html) (Accessed 7 August 2022)